MDPI

Article

Iterative Camera Calibration Method Based on Concentric Circle Grids

Liang Wei [1], Ju Huo [1,*] and Lin Yue [2]

1 School of Electrical Engineering and Automation, Harbin Institute of Technology, Harbin 150001, China; weiliangts@163.com
2 Signal and Communication Research Institute, China Academy of Railway Sciences, Beijing 100081, China; god-1982@163.com
* Correspondence: torch@hit.edu.cn

Abstract: A concentric circle target is commonly used in the vision measurement system for its detection accuracy and robustness. To enhance the camera calibration accuracy, this paper proposes an improved calibration method that utilizes concentric circle grids as the calibration target. The method involves accurately locating the imaged center and optimizing camera parameters. The imaged concentric circle center obtained by cross-ratio invariance is not affected by perspective projection, which ensures the location accuracy of the feature point. Subsequently, the impact of lens distortion on camera calibration is comprehensively investigated. The sub-pixel coordinates of imaged centers are taken into the iterative calibration method, and camera parameters are updated. Through simulations and real experiments, the proposed method effectively reduces the residual error and improves the accuracy of camera parameters.

Keywords: concentric circle; cross-ratio invariance; iterative camera calibration; lens distortion

1. Introduction

Camera calibration is a crucial technology in the fields of vision measurement [1–5], robot navigation [6–11], and 3D reconstruction [12–16]. To acquire precise measurement information, the accurate estimation of camera parameters is essential. Camera calibration parameters include intrinsic parameters and extrinsic parameters. Intrinsic parameters include main point coordinates, effective focal length, and distortion parameters, which represent the characteristics of the camera. Extrinsic parameters include the translation vector and rotation matrix, which represent the relative position relationship between the world coordinate system and the camera coordinate system. Schemes for calibration can be classified into two categories: self-calibration [17,18] and target-based calibration. Self-calibration methods obtain the camera parameters by establishing multivariate equations of corresponding feature points from different viewpoints. These methods are flexible and do not require calibration targets. However, they are only effective in well-textured scenes. Moreover, in scenarios where the camera motion constraint is absent, the self-calibration method is has been proven to be inadequate for engineering applications. Additionally, this approach can hardly achieve the precise sub-pixel extraction of feature points in calibration images. On the contrary, the target-based calibration method can yield reliable calibration results and can be applied to various scenes.

Calibration targets can be divided into the following three categories: 1D targets [19–21], 2D targets [22–24], and 3D targets [25,26]. The 1D target consists of several collinear points. Due to the ease of capturing feature points on the target using multiple cameras simultaneously, it is commonly used in multi-camera calibration. However, the 1D target lacks strong spatial geometric constraints, resulting in low calibration accuracy. Traditional 3D targets typically consist of two or three orthogonal planes, which aid in achieving higher calibration accuracy. However, designing such targets may be challenging and expensive.

Especially in the case of some large measurement scenes, this calibration method is more restricted by space. The sphere is used as a simple 3D target due to its strong contour continuity, which helps compensate for distortion caused by large viewing angles [27]. It is important to note that the size and distance of the sphere significantly affect calibration results. Additionally, there are only a few feature points involved in the calibration process. Compared to 1D and 3D targets, designing a 2D target is relatively easier. This is because calibration patterns can be printed on a planar board, allowing for the easy manufacturing of high-precision targets.

Zhang's chessboard calibration method [28] is considered one of the most representative 2D target-based calibration methods. This approach realizes the conversion between the world coordinate system and the image coordinate system by extracting Harris corners from chessboard images. The initial values of the camera parameters are obtained using a linear model. Subsequently, the reprojection error function is established, and the Levenberg–Marquardt algorithm is utilized for optimization. However, the detection accuracy of chessboard corner points is easily affected by image noise, distortion, and resolution. On the other hand, circular feature points offer the advantages of easy recognition and noise resistance, making them commonly employed in camera calibration and measurement [29–34]. In perspective projection, a circle is imaged as an ellipse. The projection of the space of the circle center does not coincide with the ellipse center. To address this issue, many methods have been investigated to accurately locate the imaged circle center. Jiang et al. [35] introduced a novel constructive geometric method for estimating the imaged center and optimizing it using homological constraints. The method iteratively finds the solutions without any parameter information. Nevertheless, it is important to verify the efficiency and stability of this method. Based on the characteristics of tangent lines and the Hough transform, Ying et al. [36] utilized four tangent lines of the concentric circle to determine a straight line, where the projected center is located on this line. By finding several straight lines, the intersection point of these lines can be identified as the projected center. In [37], the imaged circle center and the vanishing line were recovered by exploring the properties of the common self-polar triangle of concentric circles. But this method requires calculating the inversion and eigenvectors of the matrix. Kim et al. [38] investigated the geometric and algebraic constraints associated with the projected concentric circle. They introduced a rank-1 constraint to determine the center by solving a quartic equation. However, this approach may lead to numerical instability. And Zhang et al. [39] formulated the solution of the imaged circle center into a first-order polynomial eigenvalue problem by considering the pole–polar relationship based on the concentric circle. Compared with the previous work of Jiang, this technique reduces computation complexity. To minimize the perspective projection error, Shao et al. [40] confirmed the position of the imaged circle center by computing the eigenvectors of the concentric circle projection matrix.

The aforementioned research address the problem of center deviation of circular feature points in the linear perspective projection. However, due to lens distortion, the reprojection error function established in calibration is nonlinear [41,42]. Thus, it is crucial to consider the influence of lens distortion on calibration accuracy. Hartley [43] proposed a calibration method that takes into account radial distortion, which is rapid and not affected by the local minimum problem. While the radial component of lens distortion is dominant, it is also coupled with the tangential component, and thus both should be considered. Ricolfe-Viala [44] corrected the images and calculated the lens distortion separately from the intrinsic and extrinsic parameters of the camera. However, this algorithm is more complex. Yang et al. [41] discussed the impact of lens distortion and presented a robust geometric camera calibration method. The objective of compensation is to reduce the distance between the model and the actual position by adjusting all camera parameters. Zhao et al. [41] analyzed lens distortion in camera imaging and designed a template that consists of a line through the center of the concentric circle. Orthogonal vanishing points were utilized to solve the camera's intrinsic parameters. Additionally, they optimized

the positions of the distortion points to approach the ideal points, thereby enhancing the accuracy of camera calibration.

In the circle grids target-based calibration method, two sources affect the accuracy of camera calibration, namely the high-precision location of the circle center and the optimization of camera parameters. To address the above limitations, this paper proposes an improved camera calibration method that combines a concentric circle center location algorithm and an iterative compensation algorithm for the calibration parameters. The imaged concentric circle center obtained by cross-ratio invariance is not affected by the perspective projection, which ensures the location accuracy of the feature point. In addition, to achieve higher calibration accuracy, an iterative compensation framework is developed to refine the calibration results.

The remainder of this paper is organized as follows. Section 2 presents the concentric circle center location method, which is based on the invariance of the cross-ratio, and introduces a novel iterative approach for camera calibration that takes into account the influence of lens distortion. To validate the robustness and effectiveness of the method, simulations and practical experiments are conducted, as presented in Section 3. Section 4 discusses the differences and improvements of the proposed method. Finally, Section 5 gives the conclusion.

2. Materials and Methods

2.1. Concentric Circle Center Location Method Based on Cross-Ratio Invariance

The pinhole camera model is the most commonly used in computer vision, as shown in Figure 1. The relationship between the space point $P_w(x_w, y_w, z_w)$ in the world coordinate system and the projection point $P_u(u, v)$ on the image plane can be expressed as follows [28]:

$$s \begin{bmatrix} u \\ v \\ 1 \end{bmatrix} = K\begin{bmatrix} R & T \end{bmatrix} \begin{bmatrix} x_w \\ y_w \\ z_w \\ 1 \end{bmatrix} = \begin{bmatrix} f_u & 0 & u_0 & 0 \\ 0 & f_v & v_0 & 0 \\ 0 & 0 & 1 & 0 \end{bmatrix} \begin{bmatrix} R & T \\ 0 & 1 \end{bmatrix} \begin{bmatrix} x_w \\ y_w \\ z_w \\ 1 \end{bmatrix}. \tag{1}$$

where, s is a scale factor; K is the intrinsic parameter matrix of the camera; f_u, f_v denote the focal length coordinate of the camera; (u_0, v_0) is the principal point coordinate of the camera; and R and T respectively represent a 3×3 rotation matrix and a 3×1 translation vector between the world coordinate system and the camera coordinate system.
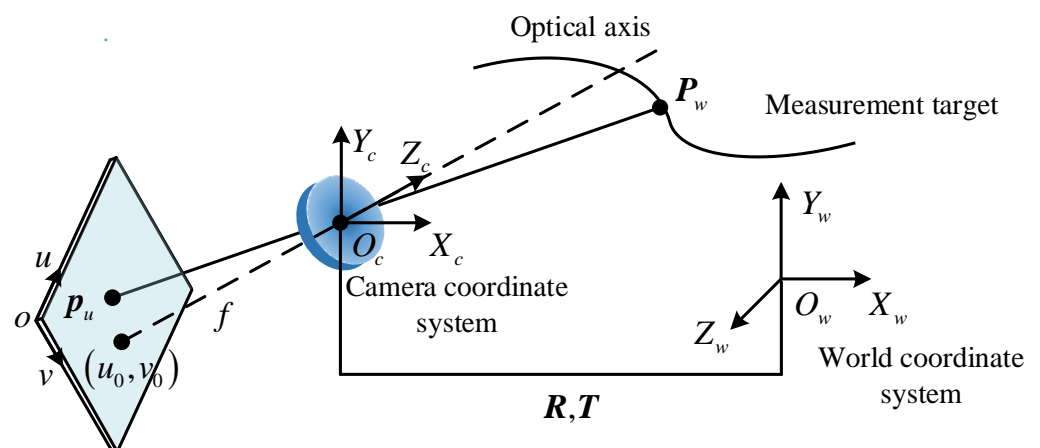

Figure 1. Pinhole camera model.

The coordinate of the feature point on the planar calibration target $z_w = 0$, let us use r_i to denote the i-th column of the rotation matrix R. According to Equation (1), we have:

$$s \begin{bmatrix} u \\ v \\ 1 \end{bmatrix} = K \begin{bmatrix} r_1 & r_2 & r_3 & T \end{bmatrix} \begin{bmatrix} x_w \\ y_w \\ 0 \\ 1 \end{bmatrix} = K \begin{bmatrix} r_1 & r_2 & T \end{bmatrix} \begin{bmatrix} x_w \\ y_w \\ 1 \end{bmatrix}. \tag{2}$$

Therefore, Equation (2) can be expressed as:

$$s \begin{bmatrix} u \\ v \\ 1 \end{bmatrix} = H \begin{bmatrix} x_w \\ y_w \\ 1 \end{bmatrix} = \begin{bmatrix} h_{11} & h_{12} & h_{13} \\ h_{21} & h_{22} & h_{23} \\ h_{31} & h_{32} & h_{33} \end{bmatrix}^{-1} \begin{bmatrix} x_w \\ y_w \\ 1 \end{bmatrix}. \tag{3}$$

where, H is a homography matrix, $H = K \begin{bmatrix} r_1 & r_2 & T \end{bmatrix}$.

On the planar target, let the circle center be at the origin of the world coordinate system and r be the radius. Then, the circle can be represented in the matrix form as:

$$C = \begin{bmatrix} 1 & 0 & 0 \\ 0 & 1 & 0 \\ 0 & 0 & -r^2 \end{bmatrix} \tag{4}$$

In the perspective projection, the circle is imaged into an ellipse, we have:

$$sE = H^{-T} C H^{-1}. \tag{5}$$

where, $E = \begin{bmatrix} A & C/2 & D/2 \\ C/2 & B & E/2 \\ D/2 & E/2 & F \end{bmatrix}$ is the conic coefficient matrix of the ellipse.

According to Equations (3)–(5), the parameters of the conic coefficient matrix can be obtained:

$$\begin{aligned}
A &= h_{11}{}^2 + h_{21}{}^2 - h_{31}{}^2 r^2 \\
B &= h_{12}{}^2 + h_{22}{}^2 - h_{32}{}^2 r^2 \\
C &= 2\left(h_{11}h_{12} + h_{21}h_{22} - h_{31}h_{32}r^2\right) \\
D &= 2\left(h_{11}h_{13} + h_{21}h_{23} - h_{31}h_{33}r^2\right) \\
E &= 2\left(h_{12}h_{13} + h_{22}h_{23} - h_{32}h_{33}r^2\right) \\
F &= h_{13}{}^2 + h_{23}{}^2 - h_{33}{}^2 r^2
\end{aligned} \tag{6}$$

And the ellipse center (e_x, e_y) is:

$$\begin{aligned}
e_x &= (CE - 2BD)/\left(4AB - C^2\right) = \left(m_1 r^2 + n_1\right)/\left(m r^2 + n\right) \\
e_y &= (CD - 2AE)/\left(4AB - C^2\right) = \left(m_2 r^2 + n_2\right)/\left(m r^2 + n\right)
\end{aligned}. \tag{7}$$

The factors m, m_1, m_2, n, n_1, n_2 can be calculated with the parameters in the homography matrix H. When r is set to 0, let (c_x, c_y) be the imaged circle center. The slope k of the straight line determined by (e_x, e_y) and (c_x, c_y) can be calculated as follows:

$$k = \frac{e_y - c_y}{e_x - c_x} = \frac{m_2 n - n_2 m}{m_1 n - n_1 m} \tag{8}$$

In Equation (8), k is a constant that is not related to the radii of the circle. Therefore, the centers of the ellipses projected by concentric circles and the imaged centers are collinear points.

Figure 2 shows a concentric circle feature point and the projection on the image plane. P_u^{e1}, P_u^{e2} represent the centers of two ellipses, and P_u is the projection of the concen-

tric circle center P_w. A line l_u is established connecting P_u, P_u^{e1}, P_u^{e2}, and this line intersects both ellipses at four different points P_u^1, P_u^2, P_u^3, and P_u^4. Based on the characteristics of projective geometry, there is a line l_w that passes through P_w and intersects the concentric circle at four points P_w^1, P_w^2, P_w^3, and P_w^4. P_w^∞ is the vanishing point on the line l_w. Additionally, $P_w^1, P_w^2, P_w^3, P_w^4, P_w^\infty$ demonstrate the perspective projection relationship with $P_u^1, P_u^2, P_u^3, P_u^4, P_u^\infty$.
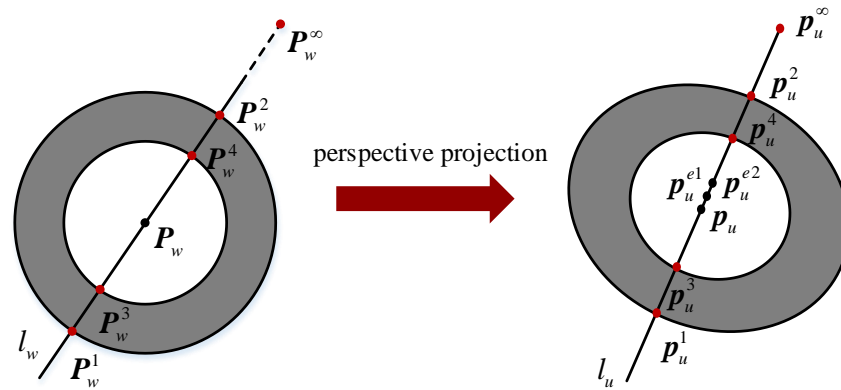

Figure 2. Concentric circle feature point.

With the properties of the harmonic conjugated points, the cross-ratio equations can be developed as follows:

$$\left(P_w^1, P_w^2; P_w, P_w^\infty\right) = \left(P_w^3, P_w^4; P_w, P_w^\infty\right) = -1. \tag{9}$$

Because the cross-ratio remains unchanged under projective transformation, we obtain:

$$\left(P_u^1, P_u^2; P_u, P_u^\infty\right) = \left(P_u^3, P_u^4; P_u, P_u^\infty\right) = -1. \tag{10}$$

In Equation (10), $P_u^1, P_u^2, P_u^3, P_u^4$ can be obtained by solving equations of the line and ellipses, and P_u is the imaged center. We choose the point that lies inside the concentric circle as the imaged center. In the perspective projection, when the image plane and the circle target plane are not parallel, a circle is imaged as an ellipse. There is a deviation between the ellipse center and the projection of the circle center, which is called the eccentricity error. The eccentricity error is only related to the angle between the image plane and the target plane. Figure 3 shows the mathematical model of the concentric circle; r_{in}, r_{out} are the radius of the concentric circle; $err = \left\|P_u - P_u^{e1}\right\|$ is the eccentricity error of the concentric circle.
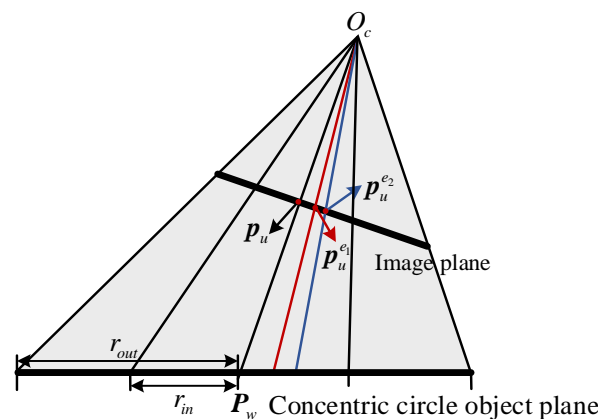

Figure 3. Mathematical model of the concentric circle.

The process of locating the imaged center of a concentric circle can be summarized in the following steps:

(I) Apply the sub-pixel edge detection algorithm to fit the projection conics and estimate the coefficient matrices.

Traditional edge detection methods include the Roberts operator, Laplace operator, Prewitt operator, and Canny operator. These methods can only locate to the pixel level and cannot meet the requirements of accurate location. To meet the high precision location requirements of the camera calibration system, we use a Canny–Zernike algorithm to detect the edge points. Firstly, the Canny operator is used to preliminarily locate the edge points. Then, the Zernike moment algorithm is applied in sub-pixel edge extraction which improves the location accuracy. The centers and coefficient matrices of ellipses are obtained using the direct least square method.

(II) Identify the intersection points between the line that traverses the ellipses' centers and the two ellipses.

Because the centers of the ellipses projected by concentric circles and the imaged centers are collinear points, we connect the two ellipses centers to establish a straight line. By combining the line equation and the projection conic equations, we obtain four intersection points.

(III) Solve the location of the imaged center according to Equation (10).

Using the principle of harmonic conjugated points and the cross-ratio invariance, the solution for the imaged center is determined.

2.2. Iterative Camera Calibration Algorithm Considering Lens Distortion

In camera calibration, the existence of lens distortion leads to the projection of a circle as a distorted ellipse, rather than a true ellipse. The center of the distorted ellipse, determined by fitting the boundary points with an ellipse, may vary from the center of the perspective ellipse. As shown in Figure 4, the distorted ellipse differs significantly from the perspective ellipse. Consequently, P_u does not coincide with the actual projection $\hat{P}_u$ of the concentric circle center.
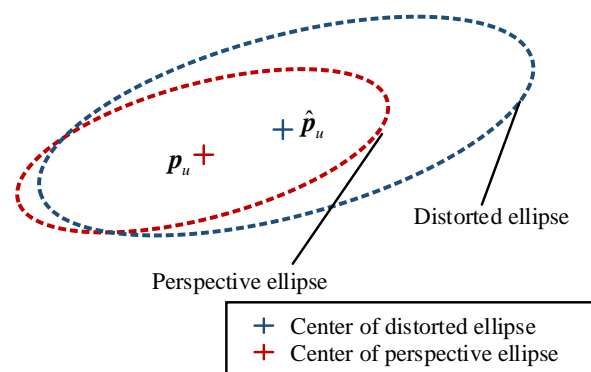

Figure 4. Difference between distorted ellipse and perspective ellipse.

The distorted image coordinate of the feature point on the normalized plane can be expressed as:

$$\begin{cases} x_d = x_c + x_c\left(k_1 r_c^2 + k_2 r_c^4\right) + 2P_1 x_c y_c + P_2\left(r_c^2 + 2x_c^2\right) \\ y_d = y_c + y_c\left(k_1 r_c^2 + k_2 r_c^4\right) + P_1\left(r_c^2 + 2y_c^2\right) + 2P_2 x_c y_c \end{cases} \tag{11}$$

where (x_c, y_c) are the undistorted image coordinate of the feature point; k_1, k_2 are the radial distortion coefficients; P_1, P_2 are the tangential distortion coefficients; $r_c^2 = x_c^2 + y_c^2$ is the distance between the image point and the principal point.

(x_c, y_c) can be calculated using:

$$\lambda \begin{bmatrix} x_c \\ y_c \\ 1 \end{bmatrix} = \begin{bmatrix} \boldsymbol{R} & \boldsymbol{T} \end{bmatrix} \begin{bmatrix} x_w \\ y_w \\ z_w \\ 1 \end{bmatrix} \tag{12}$$

Then, the real camera model can be expressed by:

$$\begin{bmatrix} u \\ v \\ 1 \end{bmatrix} = \boldsymbol{K} \begin{bmatrix} x_d \\ y_d \\ 1 \end{bmatrix}. \tag{13}$$

The Zhang calibration method involves obtaining the camera parameters through the minimization of the reprojection constraint:

$$J = \sum_{i=1}^{n} \sum_{j=1}^{m} \left\| \boldsymbol{P}_{u_{ij}} - \boldsymbol{P}'_{u_{ij}}(\boldsymbol{K}, \boldsymbol{D}, \boldsymbol{R}_i, \boldsymbol{T}_i, \boldsymbol{P}_{w_i}) \right\|^2. \tag{14}$$

where $\boldsymbol{P}_{u_{ij}}$ is the imaged center of the j-th feature point on the i-th calibration image, $i = 1, 2, \ldots, n, j = 1, 2, \ldots, m$; $\boldsymbol{P}'_{u_{ij}}(\boldsymbol{K}, \boldsymbol{D}, \boldsymbol{R}_i, \boldsymbol{T}_i, \boldsymbol{P}_{w_i})$ is the projection of the concentric circle center $\boldsymbol{P}_{w_i}$; and $\boldsymbol{D}$ represents the distortion coefficients.

The intrinsic and extrinsic parameters of the camera are first obtained by calculating the homography matrix $\boldsymbol{H}$ of several calibration images and the Levenberg–Marquardt optimization algorithm is used to solve Equation (14).

This section presents a method for iteratively adjusting the calibration parameters. Give the radius r_{in}, r_{out} and the center $\boldsymbol{P}_{w_i}$ of the concentric circle. The calibration consists of the following steps:

Step 1: Calculate the imaged concentric circle center $\boldsymbol{P}_{u_{ij}}$ and by Equation (10) and exploit the correspondence between $\boldsymbol{P}_{u_{ij}}$ and $\boldsymbol{P}_{w_i}$. According to the Zhang calibration method [28], the initial camera parameters $\boldsymbol{K}^{(0)}, \boldsymbol{D}^{(0)}$ are determined.

Step 2: Select k uniformly distributed points on each circle and calculate the projection points.

Step 3: Fit the ellipse by using the projection points that belong to the same circle and obtain the fitted concentric circle center $\left(u_{ij}^f, v_{ij}^f \right)$ according to Equation (10). Meanwhile, the projection imaged center $\left(u_{ij}^P, v_{ij}^P \right)$ of $\boldsymbol{P}_{w_i}$ is calculated using Equations (11)–(13).

Step 4: Calculate the position deviation $(\Delta u_{ij}, \Delta v_{ij})$ between $\left(u_{ij}^f, v_{ij}^f \right)$ and $\left(u_{ij}^P, v_{ij}^P \right)$, and compensate for $\boldsymbol{P}_{u_{ij}}$.

Step 5: Update the calibration values $\boldsymbol{K}, \boldsymbol{D}$ using the optimized feature points $\hat{\boldsymbol{P}}_{u_{ij}} \left(\hat{u}_{ij}, \hat{v}_{ij} \right)$.

Step 6: Continue performing Steps 2 to 5 repeatedly until the difference Δ between the two consecutive iterations is smaller than the threshold or the number of iterations reaches the maximum limit. In the iterative camera calibration algorithm, the position deviation threshold is set to 0.02 pixels and the maximum number of iterations is set to 10.

In Algorithm 1 (Pseudocode of the iterative camera calibration algorithm), we assume that there are n calibration images with m feature points on each calibration image. Camera_calibration function means the Zhang calibration method; Calculate_deviation function means the position deviation.
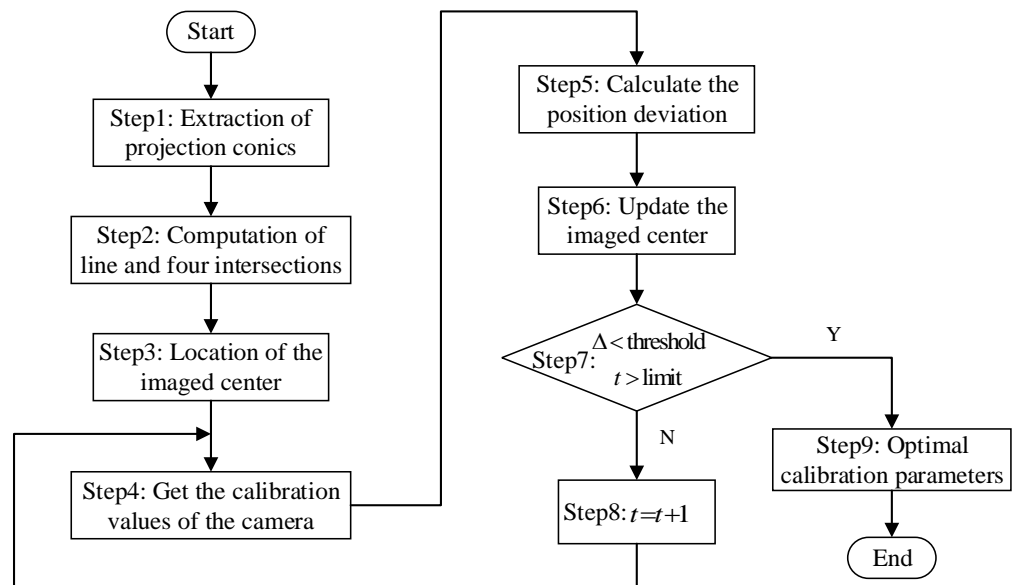

Algorithm 1. Iterative camera calibration

Input: $P_{u_{ij}}\left(u_{ij}, v_{ij}\right), P_{w_i}(x_{wi}, y_{wi}), r_{in}, r_{out}$
Output: K, D

1: $\left(K^{(0)}, D^{(0)}\right) = \text{Camera\_calibration}\left(\left(u_{ij}, v_{ij}\right), (x_{wi}, y_{wi})\right)$
2: $t \leftarrow 0, \left(\Delta u_{ij}^0, \Delta v_{ij}^0\right) \leftarrow 0, i = 1, 2, \ldots, m, j = 1, 2, \ldots, n$
3: **repeat**
4: $\left(\Delta u_{ij}^{(t+1)}, \Delta v_{ij}^{(t+1)}\right) = \text{Calculate\_deviation}\left(K^{(t)}, D^{(t)}, (x_{wi}, y_{wi}), r_{in}, r_{out}\right)$
5: $\left(\hat{u}_{ij}, \hat{v}_{ij}\right) = \left(u_{ij}, v_{ij}\right) + \left(\Delta u_{ij}^{(t+1)}, \Delta v_{ij}^{(t+1)}\right)$
6: $\left(K^{(t+1)}, D^{(t+1)}\right) = \text{Camera\_calibration}\left(\left(\hat{u}_{ij}, \hat{v}_{ij}\right), (x_{wi}, y_{wi})\right)$
7: $\Delta = \max\left(\left\|\left(\Delta u_{ij}^{(t+1)}, \Delta v_{ij}^{(t+1)}\right) - \left(\Delta u_{ij}^{(t)}, \Delta v_{ij}^{(t)}\right)\right\|\right)$
8: $t = t + 1$
9: **until** $\Delta <$ threshold or $t >$ limit
return K, D

Figure 5 shows the flow chart of the iterative camera calibration method in this paper. Firstly, we fit the projection conics of the ellipses and the line that traverses the ellipses' centers. By combining the line equation and the projection conic equations, four intersection points are calculated. Then, according to the cross-ratio invariance of collinear points, the location of the imaged centers is obtained. Furthermore, based on the Zhang calibration method, the initial camera parameters are determined. Ultimately, we calculate the position deviation and compensate for the imaged center to update the calibration values repeatedly.

Figure 5. Flow chart of the iterative camera calibration method.

In this paper, we use the concentric circle grid as the calibration target, which provides more constraints for the center location. Compared to previous research, this paper makes the following contributions. Firstly, an imaged center compensation method for concentric circles is proposed which provides a detailed description of calculating position deviation under lens distortion. Secondly, a generalized compensation framework is proposed which can refine the calibration results.

3. Experimental Results and Analysis

In this section, the advantages of the concentric circle center location method and the iterative camera calibration method are verified by simulations and actual experiments.

3.1. Synthetic Experiments

We first tested the effect of the deflection angle between the object plane and the image plane on circle center location accuracy. The camera settings were $u_0 = 1045$ pixels, $v_0 = 1010$ pixels, $f_u = 1507$ pixels, and $f_v = 1507$ pixels, and the radii of the simulation concentric circle feature point were 10mm and 20mm. The pitch angle θ_x, yaw angle θ_y and rotation angle θ_z represented the object plane deflections within the range of -1 rad to 1 rad along the x-axis, y-axis, and z-axis of the camera coordinate system, and the step was 0.1 rad. The translation vector T was set to $[0, 0, 1500]^T$ and the rotation matrix R was calculated using θ_x, θ_y, and θ_z. After selecting 10 points on each circle, based on the camera model, the projection points were calculated, which were used to fit the projection conics. Therefore, the boundary points and the fitted ellipses in the simulation images were obtained. The program was implemented in Python. The residual error between the calculated projection and the real projection of the circle center was used as the evaluation criteria to evaluate the accuracy of the location method. Figure 6a, Figure 7a, and Figure 8 show the residual error in the u and v directions by using the conventional method [34] and the proposed method.
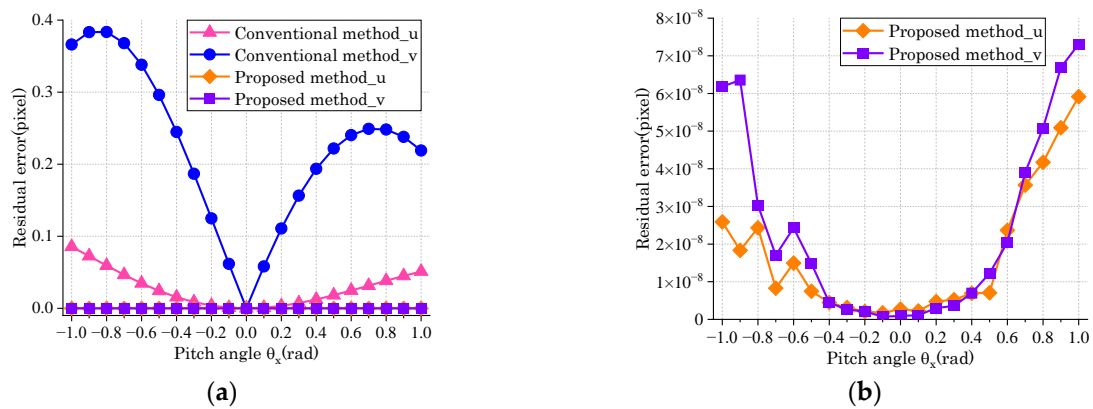
Figure 6. Effect of pitch angle on location accuracy. (**a**) The conventional and the proposed method; (**b**) enlarged view of the proposed method.
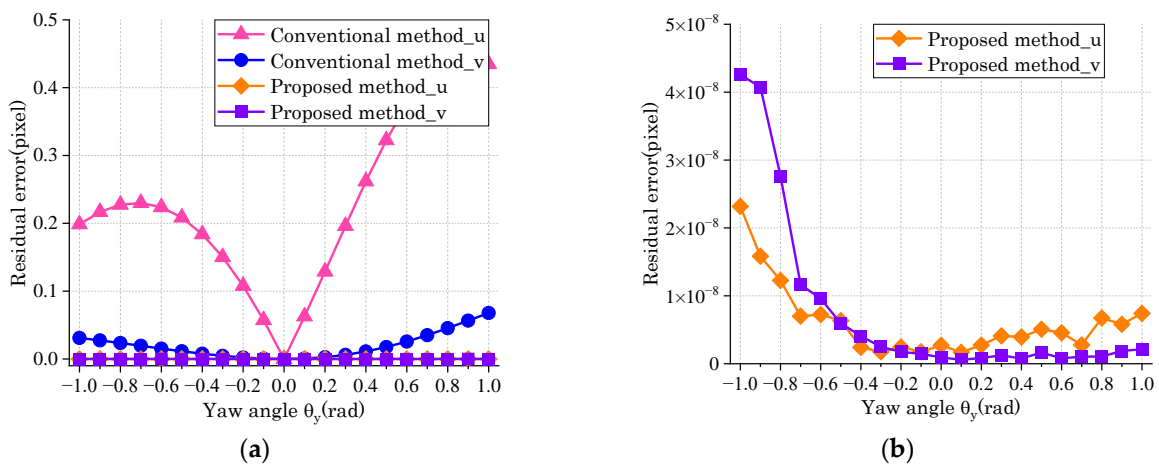
Figure 7. Effect of yaw angle on location accuracy. (**a**) The conventional and the proposed method; (**b**) enlarge view of the proposed method.
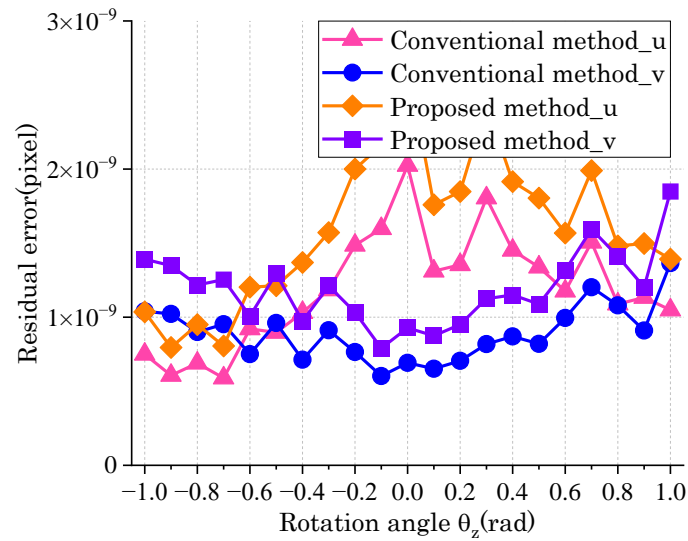
Figure 8. Effect of rotation angle on location accuracy.

As indicated in Figures 6a and 7a, the conventional method is greatly affected by the deflection angles of the object plane around the *x*-axis, *y*-axis, and the maximum residual error can reach 0.39 pixels and 0.45 pixels, respectively. Figures 6b and 7b present the residual error of the proposed method. They are independent of the deflection angle. In Figure 8, the influence of the deflection angle around the *z*-axis on the two methods can be ignored.

Subsequently, the rotation angles were all set to 1 rad. The simulated image was subjected to the addition of Gaussian noise with a mean of zero and a standard deviation that σ varies between 0 and 2 pixels. The final result was obtained by taking the average error from 100 independent experiments conducted for each noise level.

As we can see from Figure 9, the location accuracy of the two methods decreases with the increase in image noise. Compared with the conventional method, the proposed method can ensure the center location accuracy under a large rotation angle and high image noise, and the residual error of the proposed method is always less than 0.26 pixels.
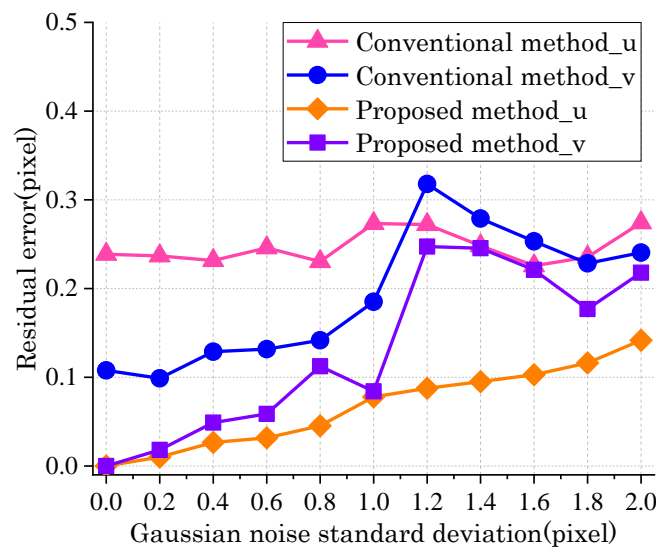

Figure 9. Effect of Gaussian noise on location accuracy.

Then, a concentric circle planar calibration target was generated. The camera parameters were kept unchanged, and the lens distortion was set at $k_1 = -0.1, k_2 = 0.08$,

$P_1 = -0.0005, P_2 = -0.0005$ as a slight distortion and at $k_1 = -0.4, k_2 = 0.3, P_1 = -0.002,$ $P_2 = -0.002$ as a heavy distortion. We simulated the calibration images under the same poses and Gaussian noise. On this basis, the Zhang method, the conventional method, and the proposed method were compared. The calibration results are listed in Tables 1 and 2. The proposed method does not exhibit a noticeable improvement effect in the presence of slight lens distortion. As the lens distortion becomes heavier, the result achieved using the proposed approach becomes more accurate.

Table 1. Results of calibration using various methods in the presence of slight lens distortion(pixel).

Parameter	Ground Truth	Zhang	Conventional	Proposed
f_x	1507	1506.989	1506.9983	1507
f_y	1507	1506.9889	1506.9952	1507
u_0	1045	1044.9253	1044.9268	1045.014
v_0	1010	1010.1394	1010.1385	1010.0848
k_1	-0.1	-0.0998	-0.1001	-0.1
k_2	0.08	0.0749	0.0823	0.08
P_1	-0.0005	-0.0005	-0.0005	-0.0005
P_2	-0.0005	-0.0005	-0.0005	-0.0005

Table 2. Results of calibration using various methods in the presence of heavy lens distortion(pixel).

Parameter	Ground Truth	Zhang	Conventional	Proposed
f_x	1507	1507.0557	1507.0552	1507
f_y	1507	1507.0402	1507.0396	1507
u_0	1045	1044.932	1044.9329	1044.9838
v_0	1010	1010.2373	1010.2359	1010.1539
k_1	-0.4	-0.3993	-0.4005	-0.4
k_2	0.3	0.2815	0.3079	0.3
P_1	-0.002	-0.002	-0.002	-0.002
P_2	-0.002	-0.002	-0.002	-0.002

3.2. Experiments with Real Images

To verify the accuracy of the circle center location method, a real template was designed, as shown in Figure 10. We show the center location results and the enlarged view. A '+' sign represents the center of the concentric circle feature point on the plane, with radii measuring 10 mm and 20 mm. The camera and the template were separated by a distance of 1500 mm, and the rotation angle was roughly 1 rad. Real images were taken using a 4M140MCX camera with a resolution of 2048×2048 pixels, the pixel size was $dx = dy = 5.5$ μm, and the focal length was $f = 12.5$ mm.
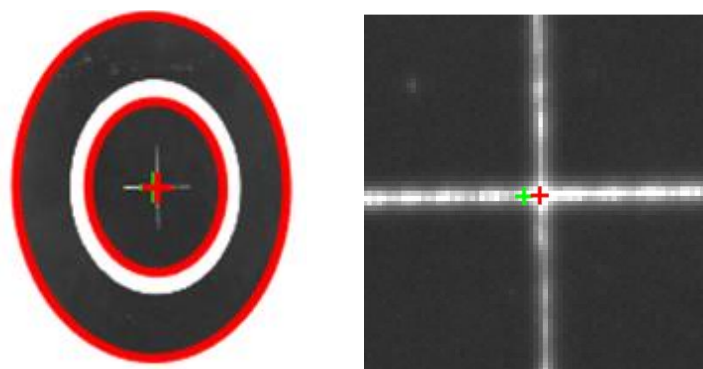
**Figure 10.** Circle center location on the real template.

In Figure 10, the conventional method is represented by the green '+' for the obtained imaged center, while the red '+' indicates the imaged center obtained using the proposed method. It can be seen that the projection determined using our approach aligned closely with the actual value.

Then, the concentric circle grid was generated on an A4 sheet of paper and pasted onto the board. The board was moved to capture images at five different poses and the intrinsic parameters are shown in Table 3.

Table 3. Evaluating intrinsic parameters using various methods in a real experiment(pixel).

Parameter	Zhang	Conventional	Proposed
f_x	2281.2359	2248.0639	2260.9497
f_y	2280.7966	2247.8106	2260.8361
u_0	1040.5597	1037.8423	1029.0437
v_0	1020.5549	1022.6404	1026.9882
k_1	-0.1532	-0.1539	-0.1544
k_2	0.0835	0.1723	0.1791
P_1	-0.0004	-0.0004	-0.0006
P_2	-0.0007	-0.0005	-0.0006

Reprojection errors are usually the evaluation standard of camera calibration accuracy. Feature points are reprojected to the image space and the reprojection errors are shown in Figure 11. The concentration of the reprojection error distribution of the proposed method is evident.

(a)

(b)

(c)
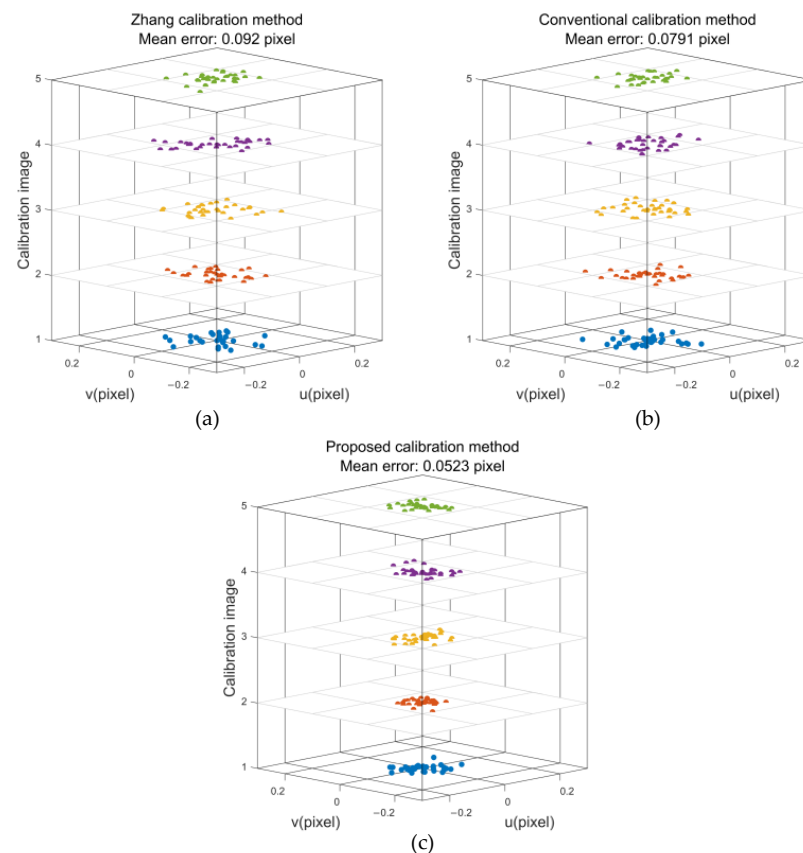
Figure 11. Reprojection errors distribution using different methods. (**a**) Reprojection errors distribution of Zhang calibration method; (**b**) Reprojection errors distribution of conventional calibration method; (**c**) Reprojection errors distribution of proposed calibration method.

The mean reprojection error for the Zhang calibration method, the conventional calibration method, and the proposed method is 0.092 pixels, 0.0791 pixels, and 0.0523 pixels, respectively. The results indicate that the proposed method offers specific benefits in enhancing the precision of calibration under the same conditions.

4. Discussion

Concentric circle targets are widely used in camera calibration due to their high detection accuracy. To improve the calibration accuracy, traditional methods mainly focus on the high-precision location of the imaged center. However, the presence of position deviation in a concentric circle caused by lens distortion was commonly ignored by previous researchers. In the proposed method, the position deviation is calculated to refine the image points iteratively thus improving the calibration accuracy. Compared with previous research, the proposed method greatly improves camera calibration accuracy and can provide more accurate camera calibration results for computer vision tasks.

5. Conclusions

This paper proposes an iterative camera calibration method that considers lens distortion by using concentric circle grids as the calibration target. The cross-ratio equations were established based on the principle of collinearity, and a designed compensation framework was used to reduce the influence of lens distortion on calibration accuracy. Simulations and real experiments confirm that the proposed method has significantly enhanced both the precision of positioning and calibration performance. In practical experiments, the proposed method demonstrates an average reprojection error of 0.0523 pixels, which is 43.15% and 33.88% less than the reprojection error obtained using the Zhang calibration method and the conventional calibration method, respectively.

Author Contributions: Writing—original draft, L.W.; writing—review and editing, J.H. and L.Y. All authors have read and agreed to the published version of the manuscript.

Institutional Review Board Statement: Not applicable.

Informed Consent Statement: Not applicable.

Data Availability Statement: Restrictions apply to the availability of the data. Data can be obtained from the first author.

Conflicts of Interest: The authors declare no conflicts of interest.

References

1. Guo, S.; Zhao, Z.; Guo, L.; Wei, M. A method for measuring the absolute position and attitude parameters of a moving rigid body using a monocular camera. *Appl. Sci.* **2023**, *13*, 11863. [CrossRef]
2. Cui, J.S.; Min, C.W.; Feng, D.Z. Research on pose estimation for stereo vision measurement system by an improved method: Uncertainty weighted stereopsis pose solution method based on projection vector. *Opt. Express* **2020**, *28*, 5470–5491. [CrossRef] [PubMed]
3. Guo, K.; Ye, H.; Gu, J.; Chen, H. A novel method for intrinsic and extrinsic parameters estimation by solving perspective-three-point problem with known camera position. *Appl. Sci.* **2021**, *11*, 6014. [CrossRef]
4. Liu, S.D.; Xing, C.C.; Zhou, G.H. Measuring precision analysis of binocular vision system in remote three-dimensional coordinate measurement. *Laser Optoelectron. Prog.* **2021**, *58*, 1415007.
5. Ibrahim, M.; Wagdy, M.; AlHarithi, F.S.; Qahtani, A.M.; Elkilani, W.S.; Zarif, S. An efficient method for document correction based on checkerboard calibration pattern. *Appl. Sci.* **2022**, *12*, 9014. [CrossRef]
6. Guan, W.P.; Huang, L.Y.; Wen, S.S.; Yan, Z.H.; Liang, W.L.; Yang, C.; Liu, Z.Y. Robot localization and navigation using visible light positioning and SLAM fusion. *J. Light. Technol.* **2021**, *39*, 7040–7051. [CrossRef]
7. Song, S.; Chandraker, M.; Guest, C.C. High accuracy monocular SFM and scale correction for autonomous driving. *IEEE Trans. Pattern Anal. Mach. Intell.* **2016**, *38*, 730–743. [CrossRef] [PubMed]
8. Li, J.S.; Chu, J.K.; Zhang, R.; Hu, H.P.; Tong, K.; Li, J. Biomimetic navigation system using a polarization sensor and a binocular camera. *J. Opt. Soc. Am. A* **2022**, *39*, 847–854. [CrossRef]

9.   Khan, M.F.; Dannoun, E.M.A.; Nofal, M.M.; Mursaleen, M. Significance of camera pixel error in the calibration process of a robotic vision system. *Appl. Sci.* **2022**, *12*, 6406. [CrossRef]

10.   Mueggler, E.; Rebecq, H.; Gallego, G.; Delbruck, T.; Scaramuzza, D. The event-camera dataset and simulator: Event-based data for pose estimation, visual odometry, and SLAM. *Int. J. Rob. Res.* **2017**, *36*, 142–149. [CrossRef]

11.   Alhmiedat, T.; Marei, A.M.; Messoudi, W.; Albelwi, S.; Bushnag, A.; Bassfar, Z.; Alnajjar, F.; Elfaki, A.O. A SLAM-Based localization and navigation system for social robots: The pepper robot case. *Machines* **2023**, *11*, 158. [CrossRef]

12.   Herrera-Granda, E.P.; Torres-Cantero, J.C.; Rosales, A.; Peluffo-Ordóñez, D.H. A comparison of monocular visual SLAM and visual odometry methods applied to 3D reconstruction. *Appl. Sci.* **2023**, *13*, 8837. [CrossRef]

13.   Cheng, T.; Li, D.G. Image reconstruction based on a single-pixel camera and left optimization. *J. Opt. Technol.* **2022**, *89*, 269–276. [CrossRef]

14.   Kim, S.; Park, Y. 3D reconstruction of celadon from a 2D image: Application to path tracing and VR. *Appl. Sci.* **2023**, *13*, 6848. [CrossRef]

15.   Xu, L.; Bai, L.; Li, L. The effect of 3D image virtual reconstruction based on visual communication. *Wirel. Commun. Mob. Comput.* **2022**, *2022*, 6404493. [CrossRef]

16.   Xu, D.; Xing, M.D.; Xia, X.G.; Sun, G.C.; Fu, J.X.; Su, T. A multi-perspective 3D reconstruction method with single perspective instantaneous target attitude estimation. *Remote Sens.* **2019**, *11*, 1277. [CrossRef]

17.   Guan, B.; Yu, Y.; Su, A.; Shang, Y.; Yu, Q. Self-calibration approach to stereo cameras with radial distortion based on epipolar constraint. *Appl. Opt.* **2019**, *58*, 8511–8521. [CrossRef] [PubMed]

18.   Sun, J.; Cheng, X.; Fan, Q. Camera calibration based on two-cylinder target. *Opt. Express* **2019**, *27*, 29319–29331. [CrossRef] [PubMed]

19.   Duan, Y.; Yu, Y.L.; Li, P.; Jiang, S.Y. High-precision camera calibration based on a 1D target. *Opt. Express* **2022**, *12*, 36873–36888. [CrossRef] [PubMed]

20.   Lv, Y.W.; Liu, W.; Xu, X.P. Methods based on 1D homography for camera calibration with 1D objects. *Appl. Opt.* **2018**, *57*, 2155–2164. [CrossRef] [PubMed]

21.   Jiang, T.; Cheng, X.; Cui, H. Calibration method for binocular vision with large FOV based on normalized 1D homography. *Optik* **2020**, *202*, 163556. [CrossRef]

22.   Yu, J.; Liu, Y.; Zhang, Z.H.; Gao, F.; Gao, N.; Meng, Z.Z.; Jiang, X.Q. High-accuracy camera calibration method based on coded concentric ring center extraction. *Opt. Express* **2022**, *30*, 42454–42469. [CrossRef] [PubMed]

23.   Yang, S.R.; Liu, M.; Yin, S.B.; Guo, Y.; Ren, Y.J.; Zhu, J.G. An improved method for location of concentric circles in vision measurement. *Measurement* **2017**, *100*, 243–251. [CrossRef]

24.   Bu, L.B.; Huo, H.T.; Liu, X.Y.; Bu, F.L. Concentric circle grids for camera calibration with considering lens distortion. *Opt. Lasers Eng.* **2021**, *140*, 106527. [CrossRef]

25.   Yin, Y.L.; Zhu, H.B.; Yang, P.; Yang, Z.H.; Liu, K.; Fu, H.W. High-precision and rapid binocular camera calibration method using a single image per camera. *Opt. Express* **2022**, *30*, 118781–118799. [CrossRef] [PubMed]

26.   Abedi, F.; Yang, Y.; Liu, Q. Group geometric calibration and rectification for circular multi-camera imaging system. *Opt. Express* **2018**, *26*, 30596–30613. [CrossRef]

27.   Zhang, X.W.; Ren, Y.F.; Zhen, G.Y.; Shan, Y.H.; Chu, C.Q.; Liang, F. Camera calibration method for solid spheres based on triangular primitives. *Precis. Eng.-J. Int. Soc. Precis. Eng. Nanotechnol.* **2020**, *65*, 91–102.

28.   Zhang, Z.Y. A flexible new technique for camera calibration. *IEEE Trans. Pattern Anal. Mach. Intell.* **2000**, *22*, 1330–1334. [CrossRef]

29.   Zhao, Z.J.; Liu, Y.C. Applications of projected circle centers in camera calibration. *Mach. Vis. Appl.* **2010**, *21*, 301–307. [CrossRef]

30.   Wei, L.; Zhang, G.Y.; Huo, J.; Xue, M.Y. Novel camera calibration method based on invariance of collinear points and pole–polar constraint. *J. Syst. Eng. Electron.* **2023**, *34*, 744–753. [CrossRef]

31.   Liang, S.X.; Zhao, Y. Camera calibration based on the common pole-polar properties between two coplanar circles with various positions. *Appl. Opt.* **2020**, *59*, 5167–5178. [CrossRef]

32.   Hao, F.; Su, J.; Shi, J.; Zhu, C.; Song, J.; Hu, Y. Conic tangents based high precision extraction method of concentric circle centers and its application in camera parameters calibration. *Sci. Rep.* **2021**, *11*, 20686. [CrossRef]

33.   Yu, Z.Y.; Shen, G.T.; Zhao, Z.Y.; Wu, Z.W.; Liu, Y. An improved method of concentric circle positioning in visual measurement. *Opt. Commun.* **2023**, *544*, 129620. [CrossRef]

34.   Cui, J.S.; Huo, J.; Yang, M. The circular mark projection error compensation in camera calibration. *Optik* **2015**, *126*, 2458–2463. [CrossRef]

35.   Jiang, G.; Quan, L. Detection of concentric circles for camera calibration. In Proceedings of the 10th IEEE International Conference on Computer Vision, Beijing, China, 17–21 October 2005.

36.   Ying, X.H.; Zha, H.B. An efficient method for the detection of projected concentric circles. In Proceedings of the 2007 IEEE International Conference on Image Processing, San Antonio, TX, USA, 16–19 September 2007.

37.   Huang, H.F.; Zhang, H.; Cheung, Y.M. The common self-polar triangle of concentric circles and its application to camera calibration. In Proceedings of the 2015 IEEE Conference on Computer Vision and Pattern Recognition, Boston, MA, USA, 7–12 June 2015.

38.   Kim, J.S.; Gurdjos, P.; Kweon, I.S. Geometric and algebraic constraints of projected concentric circles and their applications to camera calibration. *IEEE Trans. Pattern Anal. Mach. Intell.* **2005**, *27*, 637–642.

39. Zhang, B.W.; Li, Y.F.; Chen, S.Y. Concentric-circle-based camera calibration. *IET Image Process* **2012**, *6*, 870–876. [CrossRef]

40. Shao, M.W.; Dong, J.Y.; Madessa, A.H. A new calibration method for line-structured light vision sensors based on concentric circle feature. *J. Eur. Opt. Soc. Rapid Publ.* **2019**, *15*, 1. [CrossRef]

41. Yang, X.L.; Fang, S.P. Eccentricity error compensation for geometric camera calibration based on circular features. *Meas. Sci. Technol.* **2014**, *25*, 025007. [CrossRef]

42. Shen, Y.J.; Zhang, X.; Cheng, W.; Zhu, L.M. Quasi-eccentricity error modeling and compensation in vision metrology. *Meas. Sci. Technol.* **2018**, *29*, 045006. [CrossRef]

43. Hartley, R.I.; Kang, S.B. Parameter-free radial distortion correction with centre of distortion estimation. In Proceedings of the 10th IEEE International Conference on Computer Vision, Beijing, China, 17–21 October 2005.

44. Ricolfe-Viala, C.; Sanchez-Salmeron, A.J. Robust metric calibration of non-linear camera lens distortion. *Pattern Recognit.* **2010**, *43*, 1688–1699. [CrossRef]